Fermi National Accelerator Laboratory

Multidimensional Resonance Analysis of $\Lambda_c^+ \to pK^-\pi^+$

E.M. Aitala et al.

E791 Collaboration

Fermi National Accelerator Laboratory
P.O. Box 500, Batavia, Illinois 60510

December 1999

Disclaimer

This report was prepared as an account of work sponsored by an agency of the United States Government. Neither the United States Government nor any agency thereof, nor any of their employees, makes any warranty, expressed or implied, or assumes any legal liability or responsibility for the accuracy, completeness, or usefulness of any information, apparatus, product, or process disclosed, or represents that its use would not infringe privately owned rights. Reference herein to any specific commercial product, process, or service by trade name, trademark, manufacturer, or otherwise, does not necessarily constitute or imply its endorsement, recommendation, or favoring by the United States Government or any agency thereof. The views and opinions of authors expressed herein do not necessarily state or reflect those of the United States Government or any agency thereof.

Distribution

Approved for public release; further dissemination unlimited.

Copyright Notification

This manuscript has been authored by Universities Research Association, Inc. under contract No. DE-AC02-76CH03000 with the U.S. Department of Energy. The United States Government and the publisher, by accepting the article for publication, acknowledges that the United States Government retains a nonexclusive, paid-up, irrevocable, worldwide license to publish or reproduce the published form of this manuscript, or allow others to do so, for United States Government Purposes.

Multidimensional Resonance Analysis of
$\Lambda_c^+ \to pK^-\pi^+$

E. M. Aitala,[i] S. Amato,[a] J. C. Anjos,[a] J. A. Appel,[e]
D. Ashery,[n] S. Banerjee,[e] I. Bediaga,[a] G. Blaylock,[h]
S. B. Bracker,[o] P. R. Burchat,[m] R. A. Burnstein,[f] T. Carter,[e]
H. S. Carvalho,[a] N. K. Copty,[ℓ] L. M. Cremaldi,[i] C. Darling,[r]
K. Denisenko,[e] S. Devmal,[c] A. Fernandez,[k] G. F. Fox,[ℓ]
P. Gagnon,[b] C. Gobel,[a] K. Gounder,[i] A. M. Halling,[e]
G. Herrera,[d] G. Hurvits,[n] C. James,[e] P. A. Kasper,[f]
S. Kwan,[e] D. C. Langs,[ℓ] J. Leslie,[b] B. Lundberg,[e]
J. Magnin,[a] S. MayTal-Beck,[n] B. Meadows,[c]
J. R. T. de Mello Neto,[a] D. Mihalcea,[g] R. H. Milburn,[p]
J. M. de Miranda,[a] A. Napier,[p] A. Nguyen,[g]
A. B. d'Oliveira,[c,k] K. O'Shaughnessy,[b] K. C. Peng,[f]
L. P. Perera,[c] M. V. Purohit,[ℓ] B. Quinn,[i] S. Radeztsky,[q]
A. Rafatian,[i] N. W. Reay,[g] J. J. Reidy,[i] A. C. dos Reis,[a]
H. A. Rubin,[f] D. A. Sanders,[i] A. K. S. Santha,[c]
A. F. S. Santoro,[a] A. J. Schwartz,[c] M. Sheaff,[d,q]
R. A. Sidwell,[g] A. J. Slaughter,[r] M. D. Sokoloff,[c] J. Solano,[a]
N. R. Stanton,[g] R. J. Stefanski,[e] K. Stenson,[q]
D. J. Summers,[i] S. Takach,[r] K. Thorne,[e] A. K. Tripathi,[g]
S. Watanabe,[q] R. Weiss-Babai,[n] J. Wiener,[j] N. Witchey,[g]
E. Wolin,[r] S. M. Yang,[g] D. Yi,[i] S. Yoshida,[g] R. Zaliznyak,[m]
C. Zhang,[g]

Fermilab E791 Collaboration

[a] *Centro Brasileiro de Pesquisas Físicas, Rio de Janeiro RJ, Brazil*
[b] *University of California, Santa Cruz, California 95064*
[c] *University of Cincinnati, Cincinnati, Ohio 45221*
[d] *CINVESTAV, 07000 Mexico City, DF Mexico*
[e] *Fermilab, Batavia, Illinois 60510*
[f] *Illinois Institute of Technology, Chicago, Illinois 60616*

^g *Kansas State University, Manhattan, Kansas 66506*

^h *University of Massachusetts, Amherst, Massachusetts 01003*

ⁱ *University of Mississippi-Oxford, University, Mississippi 38677*

^j *Princeton University, Princeton, New Jersey 08544*

^k *Universidad Autonoma de Puebla, Puebla, Mexico*

^ℓ *University of South Carolina, Columbia, South Carolina 29208*

^m *Stanford University, Stanford, California 94305*

ⁿ *Tel Aviv University, Tel Aviv, 69978 Israel*

^o *Box 1290, Enderby, British Columbia, V0E 1V0, Canada*

^p *Tufts University, Medford, Massachusetts 02155*

^q *University of Wisconsin, Madison, Wisconsin 53706*

^r *Yale University, New Haven, Connecticut 06511*

Abstract

We present the results of a five-dimensional resonant amplitude analysis of the $\Lambda_c^+ \to pK^-\pi^+$ system based on 946 ± 38 reconstructed decays. These data were produced in 500 GeV/c π^--N interactions by Fermilab experiment E791. We report measurements of the amplitudes for Λ_c^+ decay into nonresonant $pK^-\pi^+$ and to $p\overline{K}^{*0}(890)$, $\Delta^{++}(1232)K^-$, and $\Lambda(1520)\pi^+$ and we comment on other possible resonant enhancements. This is the first complete amplitude analysis of the $\Lambda_c^+ \to pK^-\pi^+$ system. We find that $(54.8 \pm 5.5 \pm 3.5)\%$ of the decays are nonresonant, $(19.5 \pm 2.6 \pm 1.8)\%$ of the decays are via the $\overline{K}^{*0}$ resonance, $(18.0 \pm 2.9 \pm 2.9)\%$ of the decays are via the Δ^{++} resonance, and $(7.7 \pm 1.8 \pm 1.1)\%$ of the decays are via the $\Lambda(1520)$ resonance. We find evidence for an increasingly negative polarization of the Λ_c^+ baryons as a function of p_T^2, in agreement with a recent model[1] and with a related measurement[2].

Keywords: Multidimensional, Resonance, Λ_c, Polarization
PACS: 13.30 a,13.30.Eg,13.88.+e,14.20.Lq

1   Introduction

Since the discovery of charm in 1974, great progress has been made in the understanding of charm meson decays. Charm meson lifetimes, branching fractions, and resonant decays have been studied extensively[3]. While charm baryon lifetimes and branching fractions have also been measured, these measurements are not as complete, and no information is available on the amplitude analysis of any charm baryon decay system. Measurements of charm

baryon decays yield information regarding the relative importance of spectator and exchange amplitudes. The latter are thought to play a leading role in enhancing charm baryon decay rates. The most obvious components of the $\Lambda_c^+ \to pK^-\pi^+$ decays (and charge conjugate decays, which are implied throughout this paper) include the nonresonant $pK^-\pi^+$ decay as well as the $p\overline{K}^{*0}(890)$ and $\Lambda(1520)\pi^+$ two-body decays. All three of these decays can be described by spectator and W-exchange amplitudes. In lowest order, the $\Delta^{++}(1232)K^-$ decay can occur only via the exchange amplitude. Exchange amplitudes are suppressed in charm meson decays, at least at the quark level, because of helicity and form-factor effects. These effects are not expected to inhibit exchange amplitudes for charm baryons due to the three-body nature of the interaction. To understand fully this system of decays, as well as other charmed baryon decays, a complete resonant amplitude analysis is needed.

The charm baryon and its decay products carry spin and the charm baryon may be polarized upon production. Previous charm pseudoscalar meson decay analyses have studied structure in the two-dimensional space of the decay product effective masses (Dalitz plot distributions), but the spin effects just described require five kinematic variables for a complete description. While this complicates the analysis, it affords greater sensitivity to the parameters of interest. As a by-product of the analysis, the production polarization of the Λ_c^+, $\mathbf{P}_{\Lambda_c}$, is also measured. This analysis is the first five-dimensional amplitude analysis and, as such, is unique.

2   Formalism

We parameterize the observed decay rate as a function of the Λ_c^+ polarization, $\mathbf{P}_{\Lambda_c}$, and of the magnitudes and relative phases of each intermediate two-body resonance decay amplitude. We assume that the nonresonant decay is described by an amplitude that is constant across phase space. The differential decay rate $\mathrm{d}\Gamma$ (or signal density S) may be expressed as

$$\mathrm{d}\Gamma \sim S(\vec{x}) = \frac{(1 + \mathbf{P}_{\Lambda_c})}{2}(|\sum_{\mathrm{r}} B_{\mathrm{r}}(m_{\mathrm{r}})\alpha_{\mathrm{r},\frac{1}{2},\frac{1}{2}}|^2 + |\sum_{\mathrm{r}} B_{\mathrm{r}}(m_{\mathrm{r}})\alpha_{\mathrm{r},\frac{1}{2},-\frac{1}{2}}|^2)$$

$$+ \frac{(1 - \mathbf{P}_{\Lambda_c})}{2}(|\sum_{\mathrm{r}} B_{\mathrm{r}}(m_{\mathrm{r}})\alpha_{\mathrm{r},-\frac{1}{2},\frac{1}{2}}|^2 + |\sum_{\mathrm{r}} B_{\mathrm{r}}(m_{\mathrm{r}})\alpha_{\mathrm{r},-\frac{1}{2},-\frac{1}{2}}|^2) \quad (1)$$

where $\alpha_{\mathrm{r},m,\lambda_{\mathrm{p}}}$ is the complex decay amplitude for resonance r given m, the spin projection of the Λ_c on the z-axis, and λ_{p}, the proton helicity in the Λ_c rest frame.

$B_{\mathrm{r}}(m_{\mathrm{r}})$ in Equation 1 is the normalized relativistic Breit-Wigner amplitude

corrected for the centrifugal barrier[4]. Given the decay mode $\Lambda_c \to r(\to ab)c$,

$$B_{\mathrm{r}}(m_{\mathrm{r}}) = (-2|p_c||p_a|)^L \frac{F_{\Lambda_c}F_{\mathrm{r}}}{m_0^2 - m_{\mathrm{r}}^2 - im_0\Gamma_{\mathrm{r}}} \tag{2}$$

where

$$\Gamma_{\mathrm{r}} = \Gamma_0 (\frac{q}{q_0})^{2L+1} \frac{m_0}{m_{\mathrm{r}}} \frac{F_{\mathrm{r}}^2(q)}{F_{\mathrm{r}}^2(q_0)} \tag{3}$$

for resonance r of angular momentum L at the reconstructed two body mass m_{r} with the momentum q (and q_0 when $m_{\mathrm{r}} = m_0$) of a daughter particle in the resonance's rest frame, and with resonance mass and width m_0 and Γ_0 as found in Ref. [3]. Using this convention, we set $B_{\mathrm{r}}(m_{\mathrm{r}})$ for the nonresonant decay to be 1. F_L is the strong coupling factor at the appropriate decay vertex, and takes the Blatt-Weisskopf form as described in Table 1. Table 2 lists the range of the strong interaction, R_X.

Table 1
The expressions for F used in the Breit-Wigner amplitude.

L	F_L
0	1
1	$(1 + R_X^2 q^2)^{-1/2}$
2	$(9 + 3R_X^2 q^2 + R_X^4 q^4)^{-1/2}$

Table 2
The values of R used in the Breit-Wigner amplitude.

X	R_X $(\mathrm{GeV}/c^2)^{-1}$
$\overline{K}^{*0}(890)$	3.4 [5]
$\Delta^{++}(1232)$	5.22 [6]
$\Lambda(1520)$	6.29 [7]
Λ_c^+	5.07 [8]

In Tables 3–6, where the amplitudes $\alpha_{\mathrm{r,m},\lambda_{\mathrm{p}}}$ (derived using the helicity formalism described in Ref. [9]) can be seen more explicitly, the direction $(\phi_{\mathrm{r}}, \theta_{\mathrm{r}})$ is the direction of the resonance, r, in the Λ_c rest frame, using the convention

4

of Ref. [10]. The primed angles refer to the direction of one of the resonance's daughters in the resonance's rest frame. Note that the decay amplitudes for each resonance may have contributions to each of the four terms in Equation 1.
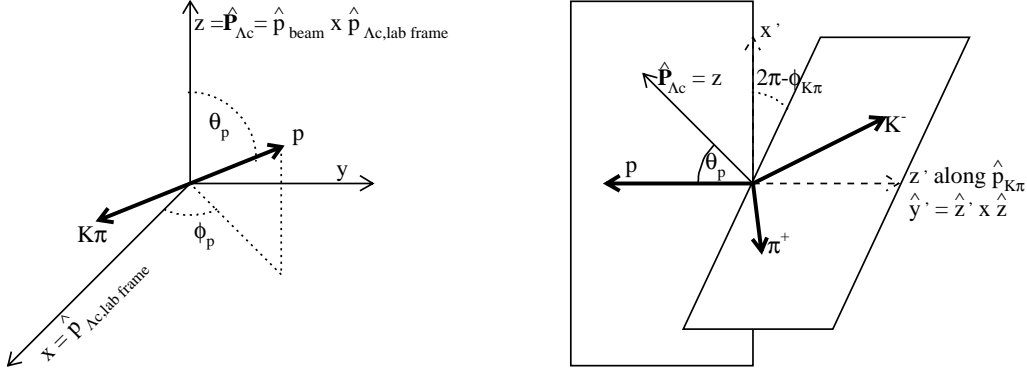

Fig. 1. Definition of angles using $\Lambda_c^+ \to p\overline{K}^{*0} \to pK^-\pi^+$ as an example. In both figures the Λ_c^+ is at rest. In the first figure, which defines (θ_p, ϕ_p), the x-axis is along the direction of motion of the Λ_c^+ in the lab frame and the z-axis is the polarization axis, normal to the plane of production. In the second figure we define $\phi_{K\pi}$ as the angle between the plane containing the $\overline{K}^{*0}$ decay products and the plane containing the proton and the x-axis.

Each event in the final data sample is described by five kinematic variables of interest (two two-body masses and the decay angles θ_p, ϕ_p, and $\phi_{K\pi}$ as defined in Figure 1) which are determined after the pKπ reconstructed mass is constrained to the Λ_c mass. We chose the quantization axis (the z-axis in the Λ_c rest frame) to be normal to the Λ_c production plane (as defined by $\hat{p}_{\text{beam}} \times \hat{p}_{\Lambda_c}$, where $\hat{p}_{\text{beam}}$ is the beam direction and $\hat{p}_{\Lambda_c}$ is the Λ_c production direction in the lab frame). The x-axis in the Λ_c rest frame is chosen to be the direction of the Λ_c in the lab frame.

3 Experiment E791 and Data Selection

We analyze data from Fermilab fixed-target experiment E791, which ran during 1991 and 1992. The data were recorded from 500 GeV/c π^- beam interactions in five thin target foils (one platinum, four diamond) whose centers were separated by about 1.53 cm. The detector, described elsewhere in more detail[11,12], was a large-acceptance, forward, two-magnet spectrometer. The key components for this study were eight planes of multiwire proportional chambers, and six planes of silicon microstrip detectors (SMD) before the target for beam tracking, a 17-plane SMD system and 35 drift chamber planes downstream of the target for track and vertex reconstruction, and two multi-cell threshold Čerenkov counters for charged particle identification.

Table 3
Amplitudes for the $\Lambda_c^+(\frac{1}{2}^+) \to (\overline{K}^{*0}(890)(1^-) \to K^-\pi^+)p(\frac{1}{2}^+)$ decay mode.

m	λ_p	Amplitude
$\frac{1}{2}$	$\frac{1}{2}$	$E_1\mathrm{e}^{i\phi_{E_1}}\,\mathrm{d}^{\frac{1}{2}}_{\frac{1}{2}\frac{1}{2}}(\theta_{\overline{\mathrm{K}}^{*0}})\,\mathrm{d}^1_{10}(\theta'_\mathrm{K})\mathrm{e}^{i\phi'_\mathrm{K}} + E_2\mathrm{e}^{i\phi_{E_2}}\,\mathrm{d}^{\frac{1}{2}}_{\frac{1}{2}-\frac{1}{2}}(\theta_{\overline{\mathrm{K}}^{*0}})\,\mathrm{d}^1_{00}(\theta'_\mathrm{K})\mathrm{e}^{i\phi_{\overline{\mathrm{K}}^{*0}}}$
$\frac{1}{2}$	$-\frac{1}{2}$	$E_3\mathrm{e}^{i\phi_{E_3}}\,\mathrm{d}^{\frac{1}{2}}_{\frac{1}{2}\frac{1}{2}}(\theta_{\overline{\mathrm{K}}^{*0}})\,\mathrm{d}^1_{00}(\theta'_\mathrm{K}) + E_4\mathrm{e}^{i\phi_{E_4}}\,\mathrm{d}^{\frac{1}{2}}_{\frac{1}{2}-\frac{1}{2}}(\theta_{\overline{\mathrm{K}}^{*0}})\,\mathrm{d}^1_{-10}(\theta'_\mathrm{K})\mathrm{e}^{i(\phi_{\overline{\mathrm{K}}^{*0}}-\phi'_\mathrm{K})}$
$-\frac{1}{2}$	$\frac{1}{2}$	$E_1\mathrm{e}^{i\phi_{E_1}}\,\mathrm{d}^{\frac{1}{2}}_{-\frac{1}{2}\frac{1}{2}}(\theta_{\overline{\mathrm{K}}^{*0}})\,\mathrm{d}^1_{10}(\theta'_\mathrm{K})\mathrm{e}^{-i(\phi_{\overline{\mathrm{K}}^{*0}}-\phi'_\mathrm{K})} + E_2\mathrm{e}^{i\phi_{E_2}}\,\mathrm{d}^{\frac{1}{2}}_{-\frac{1}{2}-\frac{1}{2}}(\theta_{\overline{\mathrm{K}}^{*0}})\,\mathrm{d}^1_{00}(\theta'_\mathrm{K})$
$-\frac{1}{2}$	$-\frac{1}{2}$	$E_3\mathrm{e}^{i\phi_{E_3}}\,\mathrm{d}^{\frac{1}{2}}_{-\frac{1}{2}\frac{1}{2}}(\theta_{\overline{\mathrm{K}}^{*0}})\,\mathrm{d}^1_{00}(\theta'_\mathrm{K})\mathrm{e}^{-i\phi_{\overline{\mathrm{K}}^{*0}}} + E_4\mathrm{e}^{i\phi_{E_4}}\,\mathrm{d}^{\frac{1}{2}}_{-\frac{1}{2}-\frac{1}{2}}(\theta_{\overline{\mathrm{K}}^{*0}})\,\mathrm{d}^1_{-10}(\theta'_\mathrm{K})\mathrm{e}^{-i\phi'_\mathrm{K}}$

Table 4
Amplitudes for the $\Lambda_c^+(\frac{1}{2}^+) \to (\Delta^{++}(1232)(\frac{3}{2}^+) \to p\pi^+)K^-$ decay mode.

m	λ_p	Amplitude
$\frac{1}{2}$	$\frac{1}{2}$	$F_1\mathrm{e}^{i\phi_{F_1}}\,\mathrm{d}^{\frac{1}{2}}_{\frac{1}{2}\frac{1}{2}}(\theta_{\Delta^{++}})\,\mathrm{d}^{\frac{3}{2}}_{\frac{1}{2}\frac{1}{2}}(\theta'_\mathrm{p}) + F_2\mathrm{e}^{i\phi_{F_2}}\,\mathrm{d}^{\frac{1}{2}}_{\frac{1}{2}-\frac{1}{2}}(\theta_{\Delta^{++}})\,\mathrm{d}^{\frac{3}{2}}_{-\frac{1}{2}\frac{1}{2}}(\theta'_\mathrm{p})\mathrm{e}^{i(\phi_{\Delta^{++}}-\phi'_\mathrm{p})}$
$\frac{1}{2}$	$-\frac{1}{2}$	$F_1\mathrm{e}^{i\phi_{F_1}}\,\mathrm{d}^{\frac{1}{2}}_{\frac{1}{2}\frac{1}{2}}(\theta_{\Delta^{++}})\,\mathrm{d}^{\frac{3}{2}}_{\frac{1}{2}-\frac{1}{2}}(\theta'_\mathrm{p})\mathrm{e}^{i\phi'_\mathrm{p}} + F_2\mathrm{e}^{i\phi_{F_2}}\,\mathrm{d}^{\frac{1}{2}}_{\frac{1}{2}-\frac{1}{2}}(\theta_{\Delta^{++}})\,\mathrm{d}^{\frac{3}{2}}_{-\frac{1}{2}-\frac{1}{2}}(\theta'_\mathrm{p})\mathrm{e}^{i\phi_{\Delta^{++}}}$
$-\frac{1}{2}$	$\frac{1}{2}$	$F_1\mathrm{e}^{i\phi_{F_1}}\,\mathrm{d}^{\frac{1}{2}}_{-\frac{1}{2}\frac{1}{2}}(\theta_{\Delta^{++}})\,\mathrm{d}^{\frac{3}{2}}_{\frac{1}{2}\frac{1}{2}}(\theta'_\mathrm{p})\mathrm{e}^{-i\phi_{\Delta^{++}}} + F_2\mathrm{e}^{i\phi_{F_2}}\,\mathrm{d}^{\frac{1}{2}}_{-\frac{1}{2}-\frac{1}{2}}(\theta_{\Delta^{++}})\,\mathrm{d}^{\frac{3}{2}}_{-\frac{1}{2}\frac{1}{2}}(\theta'_\mathrm{p})\mathrm{e}^{-i\phi'_\mathrm{p}}$
$-\frac{1}{2}$	$-\frac{1}{2}$	$F_1\mathrm{e}^{i\phi_{F_1}}\,\mathrm{d}^{\frac{1}{2}}_{-\frac{1}{2}\frac{1}{2}}(\theta_{\Delta^{++}})\,\mathrm{d}^{\frac{3}{2}}_{\frac{1}{2}-\frac{1}{2}}(\theta'_\mathrm{p})\mathrm{e}^{-i(\phi_{\Delta^{++}}-\phi'_\mathrm{p})} + F_2\mathrm{e}^{i\phi_{F_2}}\,\mathrm{d}^{\frac{1}{2}}_{-\frac{1}{2}-\frac{1}{2}}(\theta_{\Delta^{++}})\,\mathrm{d}^{\frac{3}{2}}_{-\frac{1}{2}-\frac{1}{2}}(\theta'_\mathrm{p})$

An unrestrictive, open-charm event selection based on total transverse energy seen in the calorimeters was made in real time. Offline we require all Λ_c event candidates to have a production and decay vertex longitudinally separated by at least 6 σ_l, where σ_l is the error in that separation. The tracks and vertex fits satisfy χ^2 requirements. The vertex must be formed from proton, kaon, and pion tracks identified as such by the Čerenkov particle identification system. Proton candidates are rejected when projected into regions of the detector with poor particle identification efficiency. To reject more background, we require that the magnitude of the vector sum of the transverse momenta of all the secondary tracks with respect to the flight path of the reconstructed

Table 5
Amplitudes for the $\Lambda_c^+(\frac{1}{2}^+) \to (\Lambda(1520)(\frac{3}{2}^-) \to pK^-)\pi^+$ decay mode.

m	λ_{p}	Amplitude
$\frac{1}{2}$	$\frac{1}{2}$	$H_1 e^{i\phi_{H_1}} \mathrm{d}^{\frac{1}{2}}_{\frac{1}{2}\frac{1}{2}}(\theta_{\Lambda(1520)}) \mathrm{d}^{\frac{3}{2}}_{\frac{1}{2}\frac{1}{2}}(\theta'_{\mathrm{p}}) + H_2 e^{i\phi_{H_2}} \mathrm{d}^{\frac{1}{2}}_{\frac{1}{2}-\frac{1}{2}}(\theta_{\Lambda(1520)}) \mathrm{d}^{\frac{3}{2}}_{-\frac{1}{2}\frac{1}{2}}(\theta'_{\mathrm{p}}) e^{i(\phi_{\Lambda(1520)}-\phi'_{\mathrm{p}})}$
$\frac{1}{2}$	$-\frac{1}{2}$	$-(H_1 e^{i\phi_{H_1}} \mathrm{d}^{\frac{1}{2}}_{\frac{1}{2}\frac{1}{2}}(\theta_{\Lambda(1520)}) \mathrm{d}^{\frac{3}{2}}_{\frac{1}{2}-\frac{1}{2}}(\theta'_{\mathrm{p}}) e^{i\phi'_{\mathrm{p}}} + H_2 e^{i\phi_{H_2}} \mathrm{d}^{\frac{1}{2}}_{\frac{1}{2}-\frac{1}{2}}(\theta_{\Lambda(1520)}) \mathrm{d}^{\frac{3}{2}}_{-\frac{1}{2}-\frac{1}{2}}(\theta'_{\mathrm{p}}) e^{i\phi_{\Lambda(1520)}})$
$-\frac{1}{2}$	$\frac{1}{2}$	$H_1 e^{i\phi_{H_1}} \mathrm{d}^{\frac{1}{2}}_{-\frac{1}{2}\frac{1}{2}}(\theta_{\Lambda(1520)}) \mathrm{d}^{\frac{3}{2}}_{\frac{1}{2}\frac{1}{2}}(\theta'_{\mathrm{p}}) e^{-i\phi_{\Lambda(1520)}} + H_2 e^{i\phi_{H_2}} \mathrm{d}^{\frac{1}{2}}_{-\frac{1}{2}-\frac{1}{2}}(\theta_{\Lambda(1520)}) \mathrm{d}^{\frac{3}{2}}_{-\frac{1}{2}\frac{1}{2}}(\theta'_{\mathrm{p}}) e^{-i\phi'_{\mathrm{p}}}$
$-\frac{1}{2}$	$-\frac{1}{2}$	$-(H_1 e^{i\phi_{H_1}} \mathrm{d}^{\frac{1}{2}}_{-\frac{1}{2}\frac{1}{2}}(\theta_{\Lambda(1520)}) \mathrm{d}^{\frac{3}{2}}_{\frac{1}{2}-\frac{1}{2}}(\theta'_{\mathrm{p}}) e^{-i(\phi_{\Lambda(1520)}-\phi'_{\mathrm{p}})} + H_2 e^{i\phi_{H_2}} \mathrm{d}^{\frac{1}{2}}_{-\frac{1}{2}-\frac{1}{2}}(\theta_{\Lambda(1520)}) \mathrm{d}^{\frac{3}{2}}_{-\frac{1}{2}-\frac{1}{2}}(\theta'_{\mathrm{p}}))$

Table 6
Amplitudes for the nonresonant $\Lambda_c^+(\frac{1}{2}^+) \to pK^-\pi^+$ decay mode.

m	λ_{p}	Amplitude
$\frac{1}{2}$	$\frac{1}{2}$	$N_{++} e^{i\phi_{N_{++}}}$
$\frac{1}{2}$	$-\frac{1}{2}$	$N_{+-} e^{i\phi_{N_{+-}}}$
$-\frac{1}{2}$	$\frac{1}{2}$	$N_{-+} e^{i\phi_{N_{-+}}}$
$-\frac{1}{2}$	$-\frac{1}{2}$	$N_{--} e^{i\phi_{N_{--}}}$

Λ_c candidate be ≤ 0.4 GeV/c. To eliminate reflections from $D^+ \to K^-\pi^+\pi^+$ decays and from D^+, $D_s^+ \to K^-K^+\pi^+$ decays, we remove all events whose reconstructed $K\pi\pi$ mass is within the range [1.85, 1.89] GeV/c^2 or whose reconstructed $KK\pi$ mass is within the ranges [1.85, 1.89] GeV/c^2 or [1.95, 1.99] GeV/c^2.

After this preliminary stage of the analysis, we have 998 ± 167 $\Lambda_c^+ \to pK^-\pi^+$ signal events and $107\,368\pm366$ background events. Therefore we apply further requirements in order to improve this signal in an unbiased way. This is ac-

complished by a selection on the output of an artificial neural network. The network is trained using a Monte Carlo (MC) sample of $\Lambda_c^+ \to pK^-\pi^+$ decays for signal and events from the wings of the $pK^-\pi^+$ mass distribution in data for background. The variables used in the training include all those described in the preliminary analysis above and the transverse miss distance between the primary vertex and the line of flight of the reconstructed Λ_c candidate, the scalar sum of the p_T^2 of all the secondary tracks with respect to the flight path of the reconstructed Λ_c candidate, the significance of the separation between the secondary vertex and the closest target foil edge, the calculated proper lifetime of the reconstructed Λ_c, the ratio of the distance of each of the decay tracks from the secondary vertex to its distance from the primary vertex, and the minimum and product of the three ratios.

The cut on the neural net output is chosen to maximize $N_{\mathrm{S,MC}}/\sqrt{N_{\mathrm{S,MC}} + N_{\mathrm{B}}}$ where $N_{\mathrm{S,MC}}$ is the number of MC signal events (scaled to our data size) and N_B the number of background events in the signal region. After the cut on the neural net output, 2271 real events in the $pK^-\pi^+$ mass range of [2.18, 2.38] GeV/c^2 survive, as seen in Figure 2.
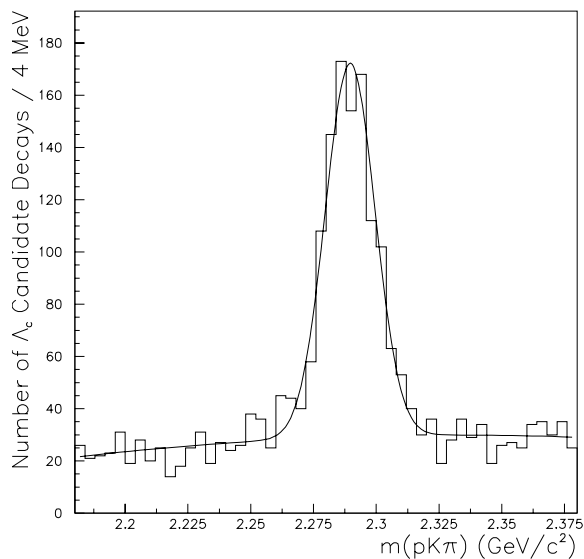

Fig. 2. $\Lambda_c \to pK\pi$ signal used in this analysis.

4   Differential Decay Rate Fit

Once the final data set is established we constrain each reconstructed $pK\pi$ mass to the mass of the Λ_c. This forces all candidate events, whether in the signal peak or in the wings, to have the same decay phase space as that of the signal. We describe each event by the five independent kinematic variables of interest (m$^2(K\pi)$, m$^2(p\pi)$, $\cos(\theta_{\mathrm{p}})$, ϕ_{p}, and $\phi_{K\pi}$).

8

Next we use an extended maximum likelihood technique to fit the data. The likelihood is assumed to have the form

$$\ln \mathcal{L} = \sum_i \ln \mathcal{L}_i - \left(\frac{1}{2} \ln \left[2\pi N_{\text{pred}} \right] + \frac{[N_{\text{pred}} - N_{\text{obs}}]^2}{2N_{\text{pred}}} \right), \qquad (4)$$

where $N_{\text{pred}} = N_{\text{S}} + N_{\text{B}}$ and N_{obs} are the predicted and observed numbers of events, and $\mathcal{L}_i$ is the likelihood of each event defined by a joint probability density in the five-dimensional phase space of the decay and the one-dimensional space of unconstrained $m_{pK\pi}$ (Fig. 2).

The likelihood for an individual event is given by

$$\mathcal{L}_i = \frac{N_S}{N_S + N_B} G(m_{pK\pi,i}, x_{\text{F}}) S(\vec{x}_i) A(\vec{x}_i) + \frac{N_B}{N_S + N_B} Q(m_{pK\pi,i}) B(\vec{x}_i) \quad (5)$$

Here G and Q represent normalized Gaussian and quadratic functions of the three body mass $m_{pK\pi}$ while $S(\vec{x})$, $A(\vec{x})$, and $B(\vec{x})$ are the signal, acceptance, and background normalized densities in the five-dimensional space of decay kinematic variables described previously. Note that the width of G is dependent on x_{F}, the scaled longitudinal momentum of the Λ_c-candidate, and is parameterized as $\sigma = \sigma_a \times x_{\text{F}} + \sigma_b$. Our x_{F} range is essentially [-0.1, +0.4]. The function $S(\vec{x})$ is described in Equation 1, while $A(\vec{x})$ is a model of the acceptance, a five-dimensional density of the reconstructed and surviving uniformly-generated MC events, and $B(\vec{x})$ is a model of the background, coming from a five-dimensional density of data events in the wings of the mass plot. We model our acceptance, $A(\vec{x})$, and background, $B(\vec{x})$, using the same approach. This common procedure is based on the K-nearest-neighbors method[13]. The K-nearest-neighbors method works on the principle that the density at a point in phase space is proportional to $N/V(r(\vec{x}_i))$ where N is the number of events which occur within volume $V(r(\vec{x}_i))$ which is a multidimensional sphere of radius r centered at $\vec{x}_i$. This method is augmented to ensure that each of the one-dimensional projections of the five-dimensional density in question ($A(\vec{x})$ and $B(\vec{x})$) matches the corresponding projection of the data set modeled (accepted MC events and background events from the data wings, respectively).

Using the fitting software, MINUIT[14], we find the parameter values which maximize $\mathcal{L}$ in Equation 4. The results can be seen in Table 7. Because the polarization is dependent on transverse momentum[1], we split the data set into three equally populated regions of p_T^2 (0.00–0.70 GeV/c, 0.70–1.24 GeV/c, and 1.24–5.20 GeV/c) and find the polarization for each region ($\mathbf{P}_{\Lambda_c,1}$, $\mathbf{P}_{\Lambda_c,2}$, and $\mathbf{P}_{\Lambda_c,3}$, respectively). The polarization versus p_T^2 is shown in Figure 3.

Figure 4 shows the one-dimensional projections of the overall fit using the parameters of Table 7 and the data in the signal region. The χ^2/DOF for the

9

Table 7

Decay amplitudes, polarization, and mass plot parameters for $\Lambda_c \to pK\pi$ from the MINUIT fit with statistical errors. The two parameters without errors are the only ones that are fixed.

| Terms	Parameter	Value
$p\overline{K}^{*0}(890)$	E_1	0.52 ± 0.17
	ϕ_{E_1}	-1.01 ± 0.48
	E_2	0.20 ± 0.10
	ϕ_{E_2}	2.35 ± 0.67
	E_3	0.21 ± 0.10
	ϕ_{E_3}	3.46 ± 0.42
	E_4	0.16 ± 0.10
	ϕ_{E_4}	5.29 ± 0.55
$\Delta^{++}(1232)K^-$	F_1	0.17 ± 0.07
	ϕ_{F_1}	4.98 ± 0.41
	F_2	0.38 ± 0.13
	ϕ_{F_2}	4.88 ± 0.40
$\Lambda^*(1520)\pi^+$	H_1	0.18 ± 0.09
	ϕ_{H_1}	5.93 ± 0.52
	H_2	0.20 ± 0.07
	ϕ_{H_2}	-0.06 ± 0.55
Nonresonant	N_{++}	0.46 ± 0.26
	$\phi_{N_{++}}$	3.48 ± 0.54
	N_{+-}	1.00
	$\phi_{N_{+-}}$	0.00
	N_{-+}	0.18 ± 0.15
	$\phi_{N_{-+}}$	0.75 ± 0.71
	N_{--}	0.94 ± 0.45
	$\phi_{N_{--}}$	1.13 ± 0.36
Polarization $[0 < p_T^2 < 0.70$ GeV/$c^2]$	$\mathbf{P}_{\Lambda_c,1}$	0.15 ± 0.21
Polarization $[0.70 < p_T^2 < 1.24$ GeV/$c^2]$	$\mathbf{P}_{\Lambda_c,2}$	-0.22 ± 0.25
Polarization $[1.24 < p_T^2 < 5.20$ GeV/$c^2]$	$\mathbf{P}_{\Lambda_c,3}$	-0.67 ± 0.15
# Signal Events	N_S	946 ± 38
# Background Events	N_B	1324 ± 43
Background Quadratic Term	b_q	-0.98 ± 10.51
Background Linear Term	b_l	1.34 ± 0.48
Λ_c Mass (GeV/c^2)	m_0	2.29 ± 0.00
Λ_c Width (MeV/c^2)	σ_a	20.1 ± 4.8
	σ_b	9.3 ± 0.6
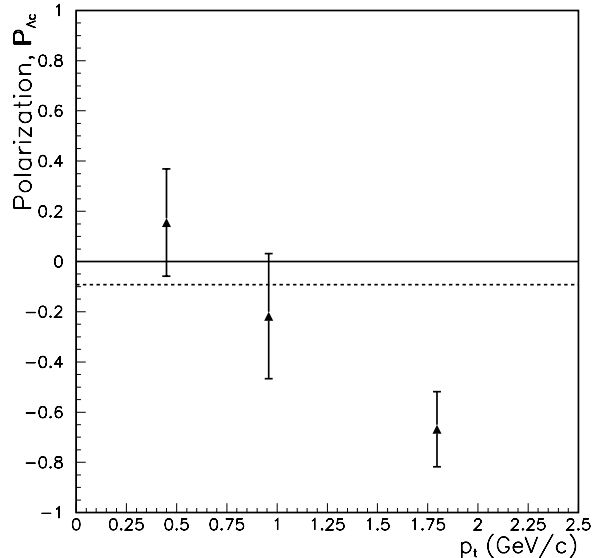
Fig. 3. The polarization of the Λ_c as a function of the Λ_c's transverse momentum. The vertical bars represent the error as found by MINUIT. They are placed at the average p_T^2 value for that region. Bin sizes are as in Table 7. The dotted line is the value of the polarization integrated over p_T^2.

agreement of the one-dimensional projections of the model and the data is 1.06. Although this agreement is reasonable, there are discrepancies, especially in the pK-mass-squared distribution. A model with a spin $\frac{1}{2}^-$ resonance decaying to pK and having a mass of 1.556±0.019 GeV/c^2 and width of 279±74 MeV/c^2 reduces the overall χ^2 of the fit. However, there is no known resonance with this description. Trying another fit model, we find some evidence for an upper tail of the $\Lambda(1405)(\to pK)$ [15]. Similarly, an improvement may be obtained by inclusion of nonresonant contributions beyond s-wave. In the case of each of these other models, the data are not sufficient to provide compelling evidence and/or to give significant measurements of the required additional parameters for the models. Figure 5 shows the one-dimensional projections of the model's resonant and nonresonant components, background, and total fit.

We calculate the fit fraction associated with each decay using Equation 6. A fit fraction F_i is the fraction of our signal described by decay via the ith contribution and is the ratio of the magnitude squared of the amplitude term describing this contribution and the complete probability of the decay:

$$F_i = \frac{\int \sum_{m,\lambda_\mathrm{p}} |B_i(m_i)\alpha_{i,m,\lambda_\mathrm{p}}|^2 \; \mathrm{d}\vec{x}}{\int \sum_{m,\lambda_\mathrm{p}} |\sum_j B_j(m_j)\alpha_{j,m,\lambda_\mathrm{p}}|^2 \; \mathrm{d}\vec{x}} \tag{6}$$

using the notation of Equation 1 where $\int \mathrm{d}\vec{x}$ implies integrating over the decay phase space.

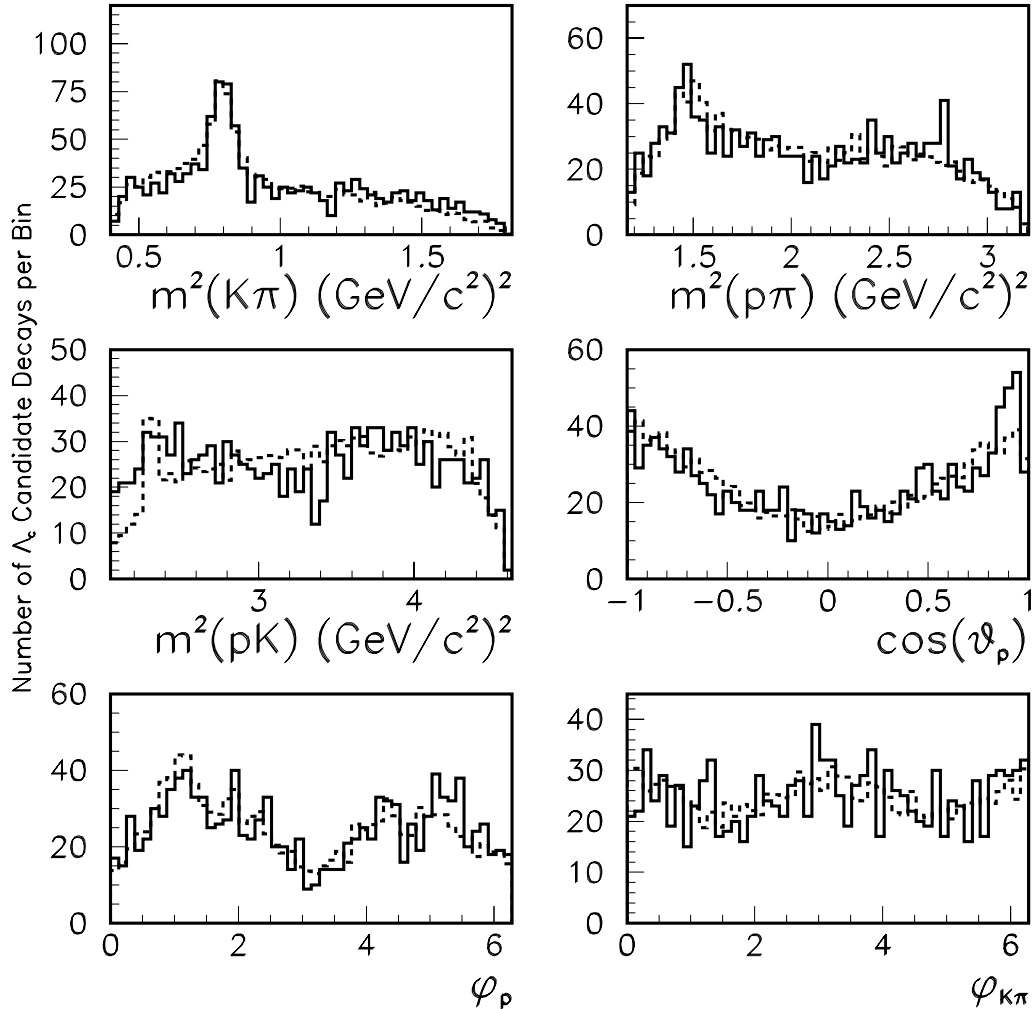The major systematic errors on the fit fractions come from uncertainties in

Fig. 4. Projections of the data within the $m_{pK\pi}$ range of (2.265 – 2.315 GeV/c^2) and overall fit superimposed. The data are shown as a solid histogram and the fits as dashed lines. There are 50 bins in each plot.

the performance of our Čerenkov counters and drift chambers, in the MC model for the production of Λ_c^+ baryons, and in the adjustment of the K-nearest-neighbors model to the one-dimensional projections. In each case, a different model of acceptance is studied and the change in the central values of parameters is taken to be an estimate of the systematic error. Table 8 lists the uncertainties in the fit fractions due to these various sources.

The fit fractions for $\Lambda_c^+ \rightarrow pK^-\pi^+$ are listed in Table 9, along with the statistical (first) and systematic (second) uncertainties. A check of these results is made by fitting the data assuming a single, average polarization. The resulting polarization is $\mathbf{P}_{\Lambda_c}$ = -0.09±0.14 (shown as the dotted line in Figure 3). The component fit fractions do not change significantly.

12
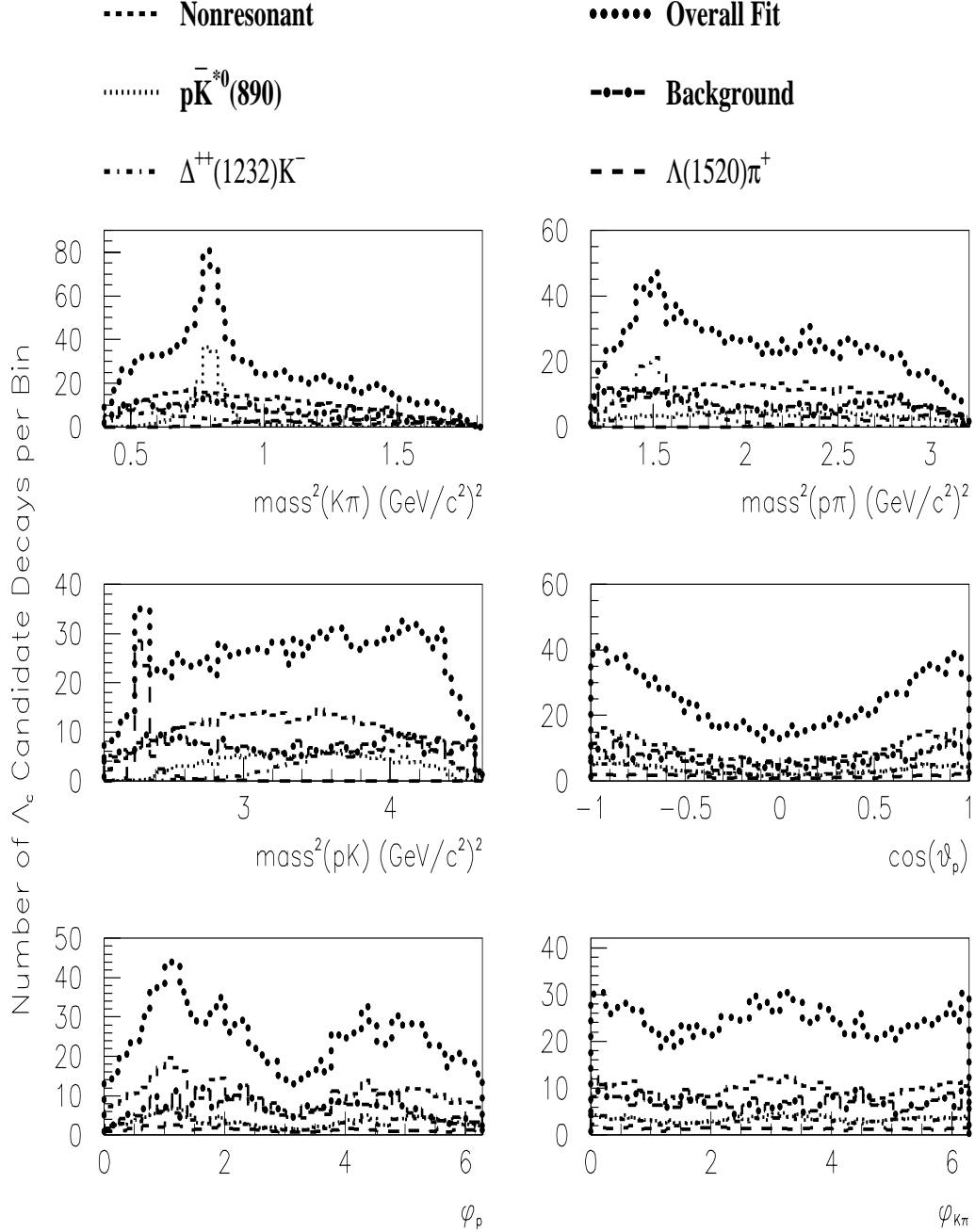
Fig. 5. Projections of the overall fit components scaled to match the number of data events within the m($pK\pi$) range of (2.265 − 2.315 GeV/c^2). There are 50 bins in each plot.

Table 8
The systematic errors on fit fractions.

Mode	Drift Chamber (%)	Čerenkov Counter (%)	Acceptance Adjust (%)	Production Model (%)	Combined Error (%)
$p\overline{K}^{*0}(890)$	1.7	0.6	0.3	0.0	1.8
$\Delta^{++}(1232)K^-$	2.5	1.2	0.7	0.1	2.9
$\Lambda(1520)\pi^+$	0.9	0.5	0.4	0.1	1.1
Nonresonant	3.2	1.1	0.9	0.1	3.5

Table 9
The fit fractions for $\Lambda_c^+ \to pK^-\pi^+$ with statistical and systematic errors from the final fit.

Mode	Fit Fraction (%)
$p\overline{K}^{*0}(890)$	19.5±2.6±1.8
$\Delta^{++}(1232)K^-$	18.0±2.9±2.9
$\Lambda(1520)\pi^+$	7.7±1.8±1.1
Nonresonant	54.8±5.5±3.5

Our results are compared to other published results in Table 10. The components in this decay do not demonstrate significant interference. This is most easily demonstrated by the fact that the fit fractions in Table 9 sum to near unity. Although we have better statistics than previous measurements, the uncertainties are comparable due to our more general fit.

Table 10
Λ_c branching ratios relative to the inclusive $\Lambda_c^+ \to pK^-\pi^+$ branching fraction. The NA32 and ISR values were calculated from one-dimensional projections only.

Mode	E791	NA32[16]	ISR[17]
$p\overline{K}^{*0}(890)$	0.29±0.04±0.03	$0.35^{+0.06}_{-0.07}$±0.03	0.42±0.24
$\Delta^{++}(1232)K^-$	0.18±0.03±0.03	$0.12^{+0.04}_{-0.05}$±0.05	0.40±0.17
$\Lambda(1520)\pi$	0.15±0.04±0.02	$0.09^{+0.04}_{-0.03}$±0.02	
Nonresonant	0.55±0.06±0.04	$0.56^{+0.07}_{-0.09}$±0.05	

5 Discussion and Conclusions

Significant resonant and non-resonant branching fractions are found in this analysis of 946 ± 38 $\Lambda_c^+ \to pK^-\pi^+$ signal events, the largest sample ever

analyzed. The size of the sample allows for inclusion of relative phases of the various contributions and a full accounting of spin and production polarization for the first time in such an analysis. The $\Delta(1232)^{++}K^-$ and $\Lambda(1520)\pi^+$ decay modes are seen as statistically significant contributions for the first time, even when uncertainties associated with phases and other variables are included. The observation of a substantial $\Delta^{++}K^-$ component provides strong evidence for the W-exchange amplitude in charm baryon decays. The observed components of the $\Lambda_c^+ \to pK^-\pi^+$ decay do not interfere significantly. Finally, we find no evidence for either $\Lambda(1600)\pi^+$ or $\Sigma(1660)\pi^+$ in the data.

In spite of the improvements in the $\Lambda_c^+ \to pK^-\pi^+$ results coming from inclusion of the newly observed contributions, there remains poor agreement between the fit and the data in the pK-mass-squared projection. Additional data from new experiments are needed in order to conclusively demonstrate additional resonances (or their tails).

We find evidence for an increasingly negative polarization of the Λ_c baryons as a function of p_T^2, in agreement with a recent model[1] and, for large negative decay asymmetry, the measurement of Ref. [2]. As suggested by the authors of the model, the assumption of T-invariance leads to further constraints on resonant phases. Again, our data are consistent with these constraints but additional data from new experiments are needed for a stringent test of CP violation.

6   Acknowledgements

References

[1] W. G. D. Dharmaratna and G. R. Goldstein, Phys. Rev. D53 (1996) 1073. See also hep-ph/9907573 by Gary R. Goldstein.

[2] M. Jezabek, K. Rybicki, and R. Rylko, Phys. Lett. B286 (1992) 175. Note that this reference has a normal to the production plane opposite to the convention adopted by their Ref. [10], by us and by Ref. [1].

[3] Particle Data Group, "Review of Particle Physics", Eur. Phys. J. C3 (1998) 1 and references therein.

[4] E687 Collaboration, P. L. Frabetti et al., Phys. Lett. B331 (1994) 217.

[5] D. Aston et al., Nucl. Phys. B296 (1988) 493.

[6] R. Koch and E. Pietarinen, Nucl. Phys. A336 (1980) 331.

[7] M. B. Watson, M. Ferro-Luzzi, and R. D. Tripp, Phys. Rev. 131 (1963) 2248.

[8] H. Pilkuhn, Relativistic Particle Physics (Springer-Verlag, New York, 1979).

[9] M. Jacob and G. C. Wick, Annals Phys. 7 (1959) 404. See also M. Perl, High Energy Hadron Physics (John Wiley & Sons, Inc., New York, 1974) and H. Pilkuhn, The Interactions of Hadrons (John Wiley & Sons, Inc., New York, 1967).

[10] J. G. Körner and H. W. Siebert, Ann. Rev. Nucl. Part. Sci. 41 (1991) 511.

[11] E791 Collaboration, E. M. Aitala et al., Phys. Lett. B371 (1996) 157 and references therein.

[12] E791 Collaboration, E. M. Aitala et al., EPJdirect C4 (1999) 1.

[13] C. M. Bishop, Neural Networks for Pattern Recognition (Clarendon Press, Oxford, 1995), p.55.

[14] F. James and M. Goossens, "MINUIT Function Minimization and Error Analysis Reference Manual", CERN Program Library Long Writeup D506, 1992.

[15] R. Dalitz in [3], p. 676.

[16] ACCMOR Collaboration, A. Bozek et al., Phys. Lett. B312 (1993) 247.

[17] Split Field Magnet Collaboration, M. Basile et al., Nuovo Cim. 62A (1981) 14.